Supporting Information

$Ba_2[FeF_4(IO_3)_2]IO_3$: a promising nonlinear optical material achieved by chemical-tailoring-induced structure evolution

Qian-Ming Huang[ab], Chun-Li Hu[a], Bing-Ping Yang[*ab], Zhi Fang[a], Yu Huang[a], Jiang-Gao Mao[*ab]

[a] State Key Laboratory of Structural Chemistry, Fujian Institute of Research on the Structure of Matter, Chinese Academy of Sciences, Fuzhou 350002, China

[b] University of Chinese Academy of Sciences, Beijing 100049, China

[*] Corresponding author (email: ybp@fjirsm.ac.cn; mjg@fjirsm.ac.cn)

Contents

Section S1 Materials and Methods

Caution: Hydrofluoric acid is highly corrosive, and personal protective equipment and standard operating procedure are required.

Reagents

Barium nitrate monohydrate ($Ba(NO_3)_2 \cdot H_2O$, AR, Aladdin), ferric oxide (Fe_2O_3, 99%, Sinopharm Chemical Reagent Co.,Ltd), ferric nitrate nonahydrate ($Fe(NO_3)_3 \cdot 9H_2O$, AR, Sinopharm Chemical Reagent Co.,Ltd), periodate (H_5IO_6, 99.9%, Aladdin), and hydrofluoric acid (HF aqueous solution, ≥40%, Aladdin) were used as received.

Syntheses

The reported two compounds were synthesized via a mild hydrothermal technology. For $Ba[FeF_4(IO_3)]$, a mixture of $Ba(NO_3)_2 \cdot H_2O$ (0.157 g, 0.60 mmol), Fe_2O_3 (0.024 g, 0.15 mmol), H_5IO_6 (0.228 g, 1.00 mmol), deionized water (2 mL), HF (0.2 mL), and HNO_3(0.15 mL) was added into a 23 mL Teflon liner, and the sealed liner was put into a stainless steel autoclave and gradually heated to 230 °C. After 72 hours of heating, the reactants were slowly cooled to room temperature at a rate of 3 °C/h. After vacuum filtering and drying, purple tabular single crystals of $Ba[FeF_4(IO_3)]$ were obtained in a high yield (60−70%, based on Fe). For $Ba_2[FeF_4(IO_3)_2]IO_3$, starting materials are $Ba(NO_3)_2 \cdot H_2O$ (0.157 g, 0.60 mmol), $Fe(NO_3)_3 \cdot 9H_2O$ (0.040 g, 0.10 mmol), H_5IO_6 (0.228 g, 1.00 mmol), H_2O (2 mL), and HF (0.15 mL); the reaction temperature was 212 °C. After cooling, washing, and drying, colorless plate-shaped $Ba_2[FeF_4(IO_3)_2]IO_3$ single crystals were collected with a high yield of 80−90% (based on Fe).

Although the two compounds were obtained via the hydrothermal synthesis approach, repeated experiments showed that there are some obvious differences in their optimal synthesis conditions. For $Ba[FeF_4(IO_3)]$, Fe_2O_3 acts as the iron source, and higher reaction temperature (230 °C) and additional nitric acid as a mineralizer are indispensable; as for $Ba_2[FeF_4(IO_3)_2]IO_3$, the reaction temperature needs to be reduced to 212 °C and the iron source was changed to soluble $Fe(NO_3)_3 \cdot 9H_2O$. Besides, the molar ratio of I/Fe is another pivotal factor. $Ba[FeF_4(IO_3)]$ crystals are formed in a relatively low I/Fe molar ratio condition while the isolation of $Ba_2[FeF_4(IO_3)_2]IO_3$ requires a higher I/Fe molar ratio, which is consistent with the relative contents of I and Fe in their crystal structures. The yields of both compounds are considerable, and the PXRDs have been

performed to check their purities (Figures S1 and S2). The existence of Ba, Fe, I, O, and F was demonstrated by EDS analysis (Figure S3).

Single-crystal structure determination

The single-crystal diffraction data were collected on a Rigaku Oxford Diffraction SuperNova CCD diffractometer (Mo Kα radiation, λ = 0.71073 Å) at about 100 K. High-quality single-crystals of the two compounds were selected for structural determination. CrysAlisPro software was used to carry out the cell refinement and data reduction. Numerical absorption correction based on Gaussian integration over a multifaceted crystal model and empirical absorption correction using spherical harmonics implemented in SCALE3 ABSPACK scaling algorithm were applied [1]. The structure was solved by the frequently-used direct method and refined by full-matrix least-squares fitting on F^2 employing the Olex 2 program with SHELX plug-in unit [2, 3]. All of the atoms of the two compounds were refined with anisotropic thermal parameters. The structures were tested for missing symmetry elements using PLATON, and none was suggested [4]. The Flack parameter of $Ba_2[FeF_4(IO_3)_2]IO_3$ was refined to 0.04(4), signifying the correctness of its absolute structure [5]. Crystallographic data and structural refinements of $Ba[FeF_4(IO_3)]$ and $Ba_2[FeF_4(IO_3)_2]IO_3$ are listed in Table S1, and some selected bond lengths and angles of them are listed in Tables S4−S7.

Powder X-ray diffraction

Powder X-ray diffraction (PXRD) analyses of the two compounds were performed on a Rigaku MiniFlex600 diffractometer equipped with a graphite monochromator (Cu Kα radiation, λ = 1.54186 Å) in the 2θ range of 10−60° with a scanning step width of 0.02°.

Energy-dispersive X-ray spectroscope

Microprobe elemental analysis was measured using a field-emission scanning electron microscope (FESEM, JSM6700F) equipped with an energy-dispersive X-ray spectroscope (EDS, Oxford INCA).

Spectroscopic measurements

Infra-red (IR) spectra were recorded on a Magna 750 FT-IR spectrometer in the form of KBr pellet in the range of 4000−400 cm^{-1}. Ultraviolet-visible-near IR (UV-vis-NIR) diffuse reflection spectra were recorded in the range of 200−2000 nm using a PerkinElmer Lambda 950 UV-vis-NIR spectrophotometer with a $BaSO_4$ powder plate used as a 100% reflectance reference. Absorption data were calculated from the diffuse-reflectance data using the Kubelka-Munk function: $\alpha/S = (1-R)^2/2R$,

where α is the absorption coefficient, S is the scattering coefficient, and R is the reflectance [6]. Extrapolation of the absorption edge to the baseline in the α/S versus energy diagram gives the band gap value.

Thermal analysis

Thermalgravimetric analyses (TGA) and differential scanning calorimetry (DSC) were performed on a NETZCH STA 449F3 thermal analyzer instrument. Powder samples were put in an Al_2O_3 crucible with an empty crucible as a reference and heated from room temperature to 1200 °C at a rate of 15 °C/min under a N_2 atmosphere.

SHG measurements

Powder SHG signals of sieved $Ba_2[FeF_4(IO_3)_2]IO_3$ samples were measured using a modified method of Kurtz and Perry [7] with laser radiation of λ = 1064 nm generated by a Q-switched Nd: YAG solid-state laser device. Pure polycrystalline $Ba_2[FeF_4(IO_3)_2]IO_3$ samples were ground and sieved into seven different particle size ranges (25–45, 45–53, 53–75, 75–105, 105–150, 150–210, >210 μm). Sieved KDP samples with the same particle-size ranges were also measured as references. Oscilloscope traces of SHG signals of $Ba_2[FeF_4(IO_3)_2]IO_3$ and KDP samples in the particle-size range of 150-210 μm were recorded.

Computational Methods

The calculations of electronic and optical properties were performed with the CASTEP code using the plane-wave pseudopotential density functional theory (DFT) [8, 9]. The generalized gradient approximation (GGA) Perdew-Burke-Ernzerhof (PBE) was selected as the exchange and correlation functional [10]. The core-electron interactions were represented by the norm-conserving pseudopotential [11]. Ba $5s^25p^66s^2$, Fe $3s^23p^63d^64s^2$, I $5s^25p^5$, O $2s^22p^4$, and F $2s^22p^5$ orbital electrons were considered as the valence electrons. A cutoff energy of 900 eV was used to determine the number of plane-wave basis sets. The Monkhorst-Pack k-point sampling of 2 × 3 × 3 was adopted to perform numerical integration over Brillouin zone for both structures. Because of the half-filled Fe-3d electronic states, the spin polarized calculations were implemented. More than 316 and 556 empty bands were used for the optical property calculations of $Ba[FeF_4(IO_3)]$ and $Ba_2[FeF_4(IO_3)_2]IO_3$, respectively. The electron localization function (ELF) diagrams (Figure S20) of both structures were also calculated to show the stereochemically active lone-pair (SALP) of I^{5+}.

Table S1. Crystallographic data and structure refinement parameters of $Ba[FeF_4(IO_3)]$ and $Ba_2[FeF_4(IO_3)_2]IO_3$.

Formula	$Ba[FeF_4(IO_3)]$	$Ba_2[FeF_4(IO_3)_2]IO_3$
Formula weight	444.09	931.23
Temperature/K	100.00(11)	99.98(15)
Crystal system	monoclinic	orthorhombic
Space group	$P2_1/c$	$Pna2_1$
a/Å	10.7066(13)	13.7239(8)
b/Å	7.5896(8)	11.4384(8)
c/Å	7.8261(8)	7.4518(6)
α/°	90	90
β/°	110.158(13)	90
γ/°	90	90
Volume/Å^3	596.99(12)	1169.78(14)
Z	4	4
ρ_{calc}/gcm^{-3}	4.941	5.288
μ/mm^{-1}	14.187	15.893
F(000)	780.0	1620.0
Radiation	MoKα (λ = 0.71073)	MoKα (λ = 0.71073)
Goodness-of-fit on F^2	1.035	1.031
Final R indexes [I>=2σ (I)]	R_1 = 0.0380, wR_2 = 0.0727	R_1 = 0.0345, wR_2 = 0.0734
Final R indexes [all data]	R_1 = 0.0511, wR_2 = 0.0813	R_1 = 0.0409, wR_2 = 0.0776
Flack parameter	N/A	0.04(4)

[a]$R_1 = \Sigma||F_o|-|F_c||/\Sigma|F_o|$; and $wR_2 = \{\Sigma[w(F_o^2-F_c^2)^2]/\Sigma[w(F_o^2)^2]\}^{1/2}$.

Table S2. Atomic coordinates ($\times 10^4$) and equivalent isotropic displacement parameters ($Å^2 \times 10^3$) for $Ba[FeF_4(IO_3)]$. U_{eq} is defined as 1/3 of the trace of the orthogonalized U_{ij} tensor.

Atoms	*x*	*y*	*z*	U(eq)
Ba1	8868.7(4)	10668.5(7)	7011.0(6)	8.86(14)
I1	5496.5(5)	8160.3(7)	3914.9(6)	8.79(15)
Fe1	7649.8(11)	5133.1(17)	6731.3(15)	8.4(3)
F1	8734(5)	4407(6)	5333(6)	14.4(11)
F2	6782(4)	2861(6)	6227(6)	12.8(10)
F3	9059(4)	3928(6)	8671(6)	10.2(10)
F4	8698(4)	7228(6)	7280(6)	11.6(10)
O1	5732(6)	8861(8)	6198(7)	11.8(12)
O2	6931(5)	9327(7)	3731(7)	10.6(12)
O3	6175(6)	6003(7)	4644(7)	11.5(13)

Table S3. Atomic coordinates ($\times 10^4$) and equivalent isotropic displacement parameters ($Å^2 \times 10^3$) for $Ba_2[FeF_4(IO_3)_2]IO_3$. U_{eq} is defined as 1/3 of the trace of the orthogonalised U_{ij} tensor.

Atom	*x*	*y*	*z*	U(eq)
Ba1	9403.8(5)	3874.3(6)	7144.4(16)	5.72(18)
Ba2	5474.0(5)	3768.2(7)	1547.1(13)	4.45(18)
I1	8765.2(5)	3720.3(6)	2139.6(14)	3.50(18)
I2	7361.6(5)	1398.6(6)	4343.4(14)	2.78(17)
I3	7424.5(5)	6134.6(6)	4323.1(16)	2.66(17)
Fe1	6526.8(12)	3786.7(13)	7047(3)	3.0(4)
F1	7422(5)	3766(6)	9048(12)	9(2)
F2	5721(5)	2636(7)	8188(11)	9.1(18)
F3	5788(5)	4924(7)	8374(11)	8.1(17)
F4	5716(5)	3947(7)	5080(13)	9.9(17)
O1	9015(6)	4930(8)	3690(14)	6.4(19)
O2	9038(6)	2543(8)	3738(13)	3.7(17)
O3	9912(6)	3731(7)	955(14)	5.3(19)
O4	6197(5)	735(7)	4789(13)	7.5(19)
O5	7007(5)	2335(7)	2509(13)	3.6(18)
O6	7408(5)	2498(8)	6152(13)	2.0(17)
O7	6262(5)	6824(8)	4781(13)	6.5(19)
O8	7041(5)	5222(7)	2460(14)	7(2)
O9	7457(5)	5056(8)	6168(13)	4.2(19)

Table S4. Selected bond lengths (Å) for $Ba[FeF_4(IO_3)]$.

Ba1-F1[3]	2.654(5)	Fe1-F1	1.930(5)
Ba1-F1[2]	3.109(5)	Fe1-F2	1.934(5)
Ba1-F1[1]	2.854(5)	Fe1-F3	1.959(4)
Ba1-F2[2]	2.682(5)	Fe1-F4	1.908(5)
Ba1-F3[1]	2.787(5)	Fe1-O2[3]	2.009(6)
Ba1-F3[2]	2.769(5)	Fe1-O3	1.955(5)
Ba1-F3[4]	2.708(4)	I1-O1	1.797(5)
Ba1-F4	2.631(5)	I1-O2	1.821(6)
Ba1-F4[1]	2.739(5)	I1-O3	1.802(6)
Ba1-O2	2.874(5)		

Symmetry transformations used to generate equivalent atoms: [1]2-X,1/2+Y,3/2-Z; [2]+X,1+Y,+Z; [3]+X,3/2-Y,1/2+Z; [4]+X,3/2-Y,-1/2+Z.

Table S5. Selected bond angles (deg.) for $Ba[FeF_4(IO_3)]$.

O1-I1-O2	95.9(3)	F2-Fe1-O3	86.4(2)
O1-I1-O3	92.9(3)	F3-Fe1-O2[3]	83.7(2)
O3-I1-O2	102.0(2)	F4-Fe1-F1	86.8(2)
F1-Fe1-F2	88.3(2)	F4-Fe1-F2	173.3(2)
F1-Fe1-F3	81.56(19)	F4-Fe1-F3	88.8(2)
F1-Fe1-O2[3]	165.1(2)	F4-Fe1-O2[3]	90.5(2)
F1-Fe1-O3	95.3(2)	F4-Fe1-O3	98.6(2)
F2-Fe1-F3	86.0(2)	O3-Fe1-F3	171.9(2)
F2-Fe1-O2[3]	93.1(2)	O3-Fe1-O2[3]	99.6(2)

Symmetry transformations used to generate equivalent atoms: [1]2-X,1/2+Y,3/2-Z; [2]+X,1+Y,+Z; [3]+X,3/2-Y,1/2+Z.

Table S6. Selected bond lengths (Å) for $Ba_2[FeF_4(IO_3)_2]IO_3$.

Ba2-O5	2.763(7)	Ba1-O6	3.245(8)
Ba2-F1[1]	3.258(8)	Ba1-O1	2.891(10)
Ba2-O8	2.804(8)	Ba1-O1[6]	2.814(8)
Ba2-F3[2]	2.664(7)	Ba1-O2	3.000(9)
Ba2-F3[1]	2.742(8)	I1-O3	1.805(9)
Ba2-F4	2.660(9)	I1-O1	1.834(9)
Ba2-F4[2]	3.272(7)	I1-O2	1.835(9)
Ba2-F2[1]	2.838(8)	I3-O8	1.814(9)
Ba2-O3[3]	2.995(8)	I3-O9	1.848(9)
Ba2-O7[2]	2.806(8)	I3-O7	1.811(7)
Ba2-O2[3]	2.968(8)	I2-O5	1.804(9)
Ba1-F1	3.070(7)	I2-O4	1.798(8)
Ba1-O9	3.082(8)	I2-O6	1.844(9)
Ba1-F2[4]	2.621(7)	Fe1-F1	1.931(8)
Ba1-O3[5]	2.927(10)	Fe1-F3	1.921(7)
Ba1-O3[6]	3.028(8)	Fe1-O9	2.041(8)
Ba1-O4[7]	3.016(9)	Fe1-F4	1.850(9)
Ba1-O4[4]	3.057(8)	Fe1-F2	1.915(7)
Ba1-O7[8]	3.193(9)	Fe1-O6	2.020(8)

Symmetry transformations used to generate equivalent atoms: [1]+X,+Y,-1+Z; [2]1-X,1-Y,-1/2+Z; [3]-1/2+X,1/2-Y,+Z; [4]1/2+X,1/2-Y,+Z; [5]+X,+Y,1+Z; [6]2-X,1-Y,1/2+Z; [7]3/2-X,1/2+Y,1/2+Z; [8]3/2-X,-1/2+Y,1/2+Z.

Table S7. Selected bond angles (deg.) for $Ba_2[FeF_4(IO_3)_2]IO_3$.

F3-Fe1-F1	87.0(3)	O6-Fe1-O9	92.2(4)
F3-Fe1-O9	90.8(3)	O3-I1-O1	98.1(4)
F3-Fe1-O6	168.3(4)	O3-I1-O2	98.4(4)
F4-Fe1-F1	174.6(3)	O1-I1-O2	95.9(4)
F4-Fe1-F3	91.4(3)	O8-I3-O9	101.1(4)
F4-Fe1-O9	93.0(3)	O7-I3-O8	98.0(4)
F4-Fe1-F2	94.1(3)	O7-I3-O9	99.9(4)
F4-Fe1-O6	99.8(4)	O5-I2-O6	99.2(4)
F2-Fe1-F1	90.9(3)	O4-I2-O5	98.6(4)
F2-Fe1-F3	86.0(3)	O4-I2-O6	100.6(4)
F2-Fe1-O9	172.3(4)	F1-Fe1-O9	81.9(3)
F2-Fe1-O6	89.5(3)	F1-Fe1-O6	82.2(3)

Table S8. Calculated dipole moments of $Ba_2[FeF_4(IO_3)_2]IO_3$ within an unit cell (Z = 4).

Polar units	Dipole moment (D = Debye)			
	x	*y*	*z*	Total magnitude
FeO_2F_4 (1)	1.269	-0.562	2.915	3.229
FeO_2F_4 (2)	-1.269	-0.562	2.915	3.229
FeO_2F_4 (3)	1.269	0.562	2.915	3.229
FeO_2F_4 (4)	-1.269	0.562	2.915	3.229
$I1O_3$ (1)	-12.614	-0.291	7.494	14.680
$I1O_3$ (2)	12.614	-0.291	7.494	14.680
$I1O_3$ (3)	-12.614	0.291	7.494	14.680
$I1O_3$ (4)	12.614	0.291	7.494	14.680
$I2O_3$ (1)	-11.286	-8.135	1.193	13.960
$I2O_3$ (2)	11.282	-8.138	1.193	13.960
$I2O_3$ (3)	-11.286	8.135	1.193	13.960
$I2O_3$ (4)	11.282	8.138	1.193	13.960
$I3O_3$ (1)	-11.011	7.422	1.299	13.340
$I3O_3$ (2)	11.011	7.422	1.299	13.340
$I3O_3$ (3)	-11.011	-7.422	1.299	13.340
$I3O_3$ (4)	11.011	-7.4222	1.299	13.340
Net dipole moment	0	0	51.604	51.604

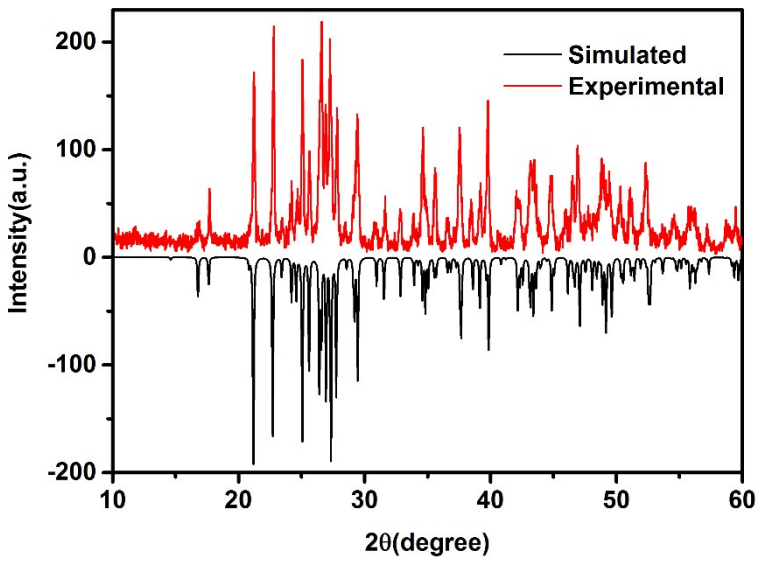

Figure S1. Simulated and experimental PXRD patterns of $Ba[FeF_4(IO_3)]$.

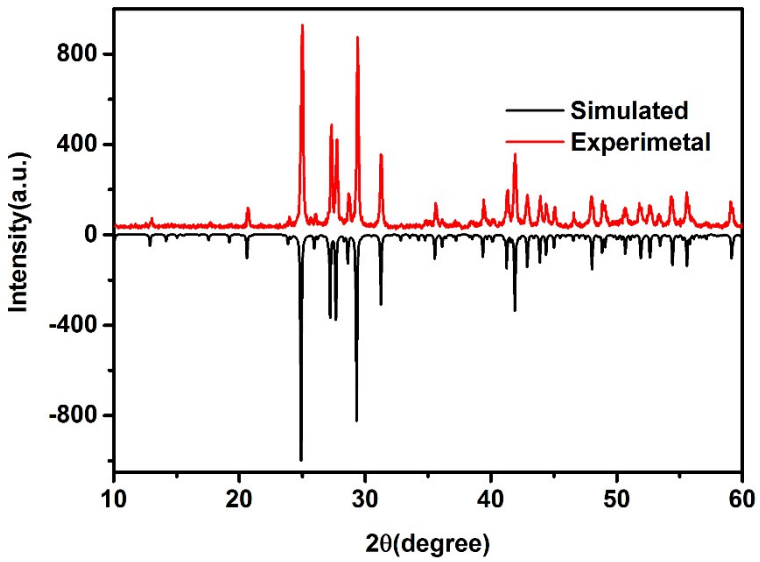

Figure S2. Simulated and experimental PXRD patterns of $Ba_2[FeF_4(IO_3)_2]IO_3$.

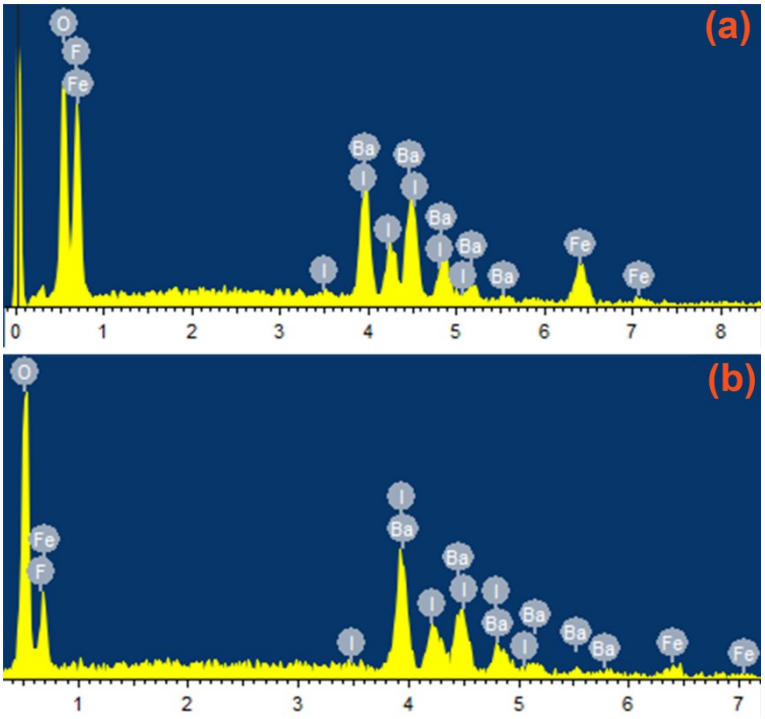

Figure S3. EDS spectra of (a) $Ba[FeF_4(IO_3)]$ and (b) $Ba_2[FeF_4(IO_3)_2]IO_3$.

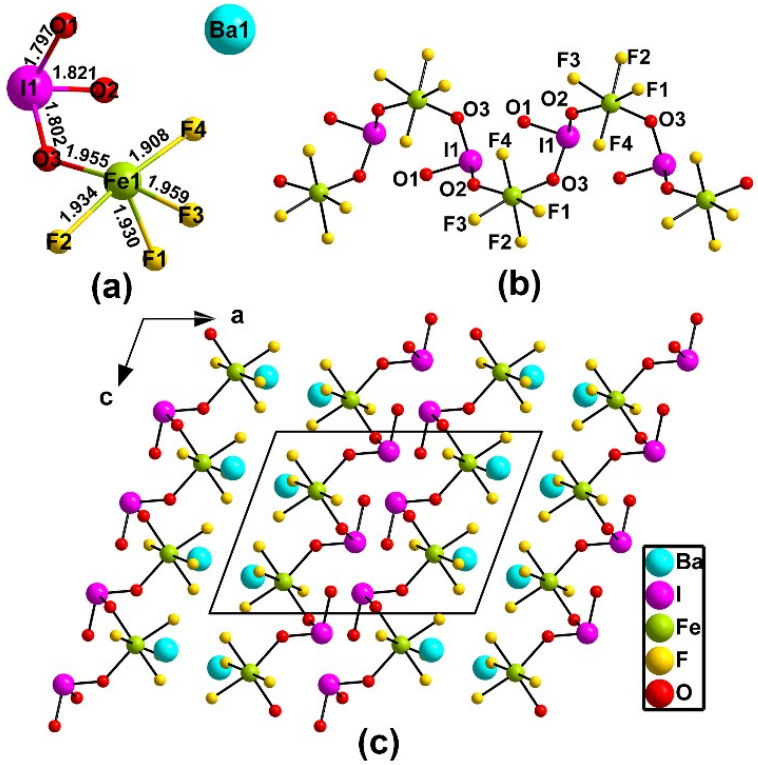

Figure S4. View of the (a) asymmetric unit of $Ba[FeF_4(IO_3)]$ and (b) 1D $[FeF_4(IO_3)]^{2-}$ zigzag polyanion chain. (c) Three-dimensional structure of $Ba[FeF_4(IO_3)]$ along the [010] direction.

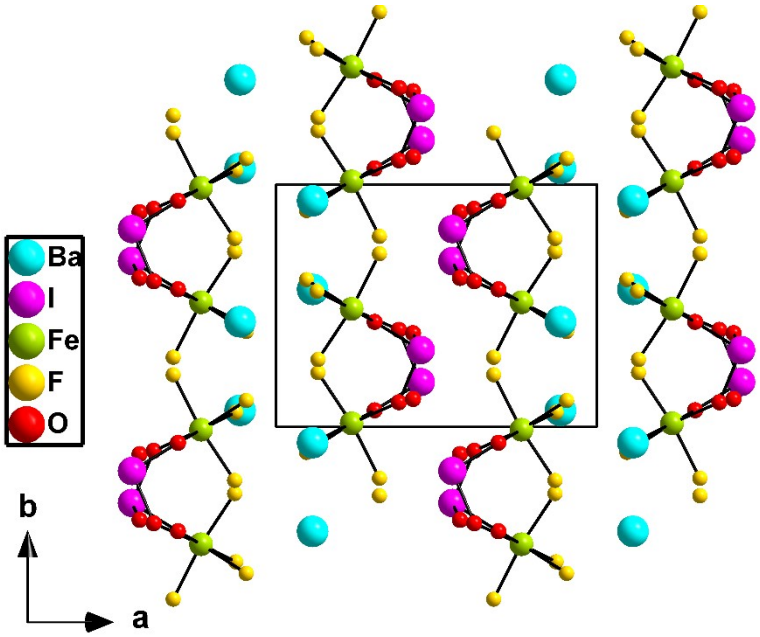

Figure S5. Overall structure of Ba[$FeF_4(IO_3)$] along the [001] direction.

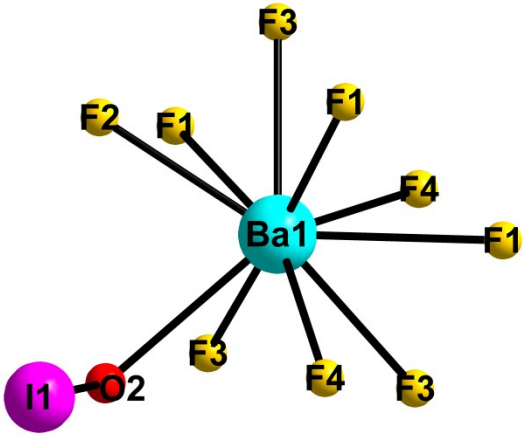

Figure S6. Coordination environments of Ba(1) of Ba[$FeF_4(IO_3)$].

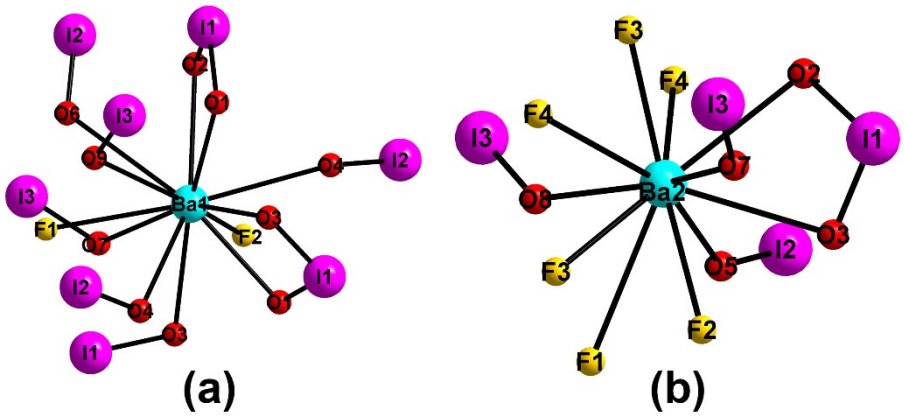

Figure S7. Coordination environments of Ba(1) and Ba(2) of $Ba_2[FeF_4(IO_3)_2]IO_3$.

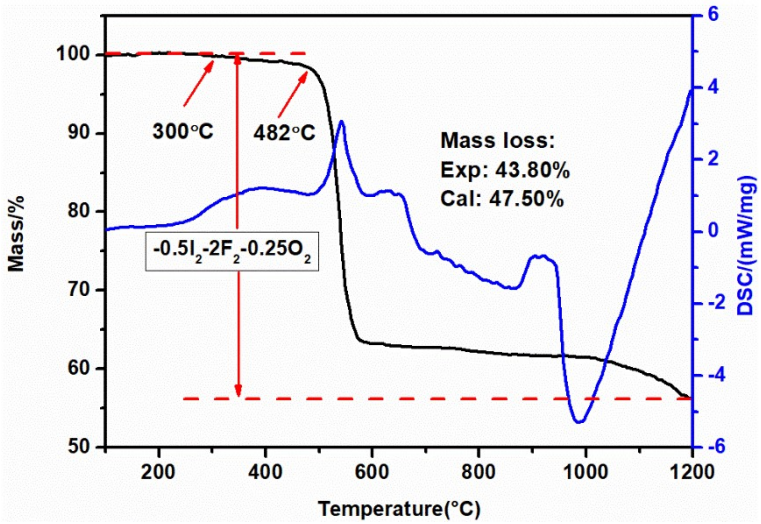

Figure S8. TGA and DSC curves of $Ba[FeF_4(IO_3)]$ under a N_2 atmosphere.

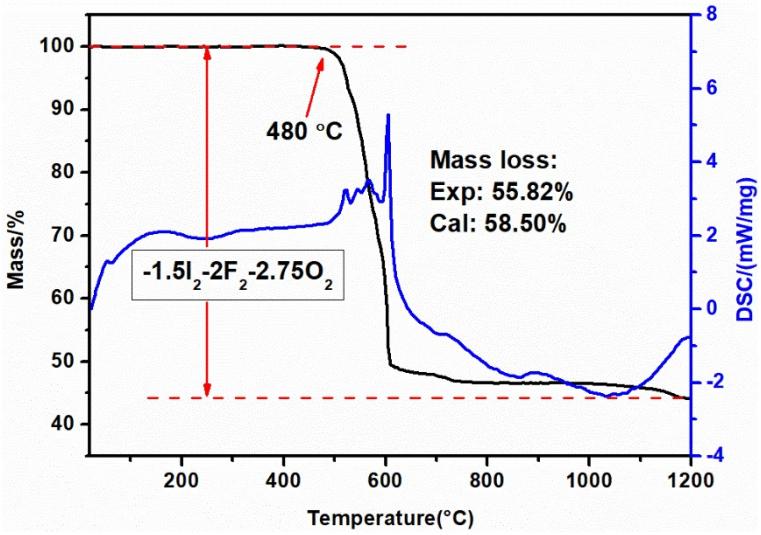

Figure S9. TGA and DSC curves of $Ba_2[FeF_4(IO_3)_2]IO_3$ under a N_2 atmosphere.

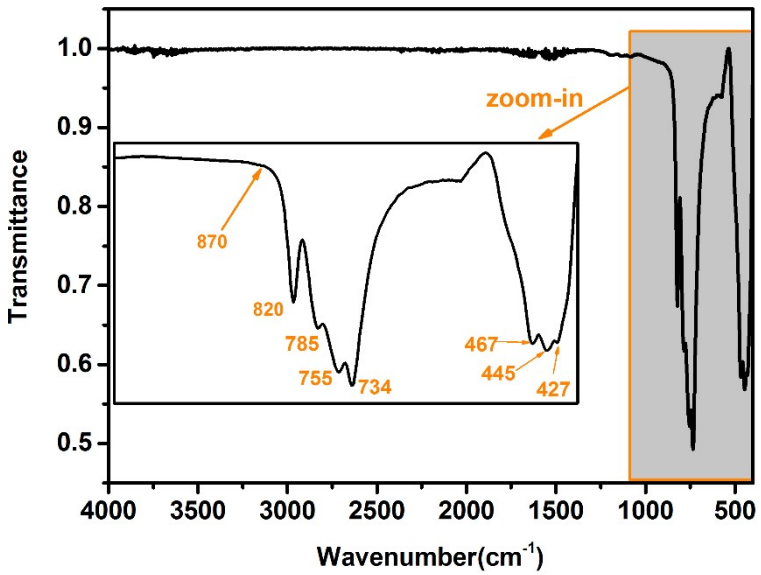

Figure S10. IR spectrum of $Ba[FeF_4(IO_3)]$, inset: zoomed-in view of IR bands.

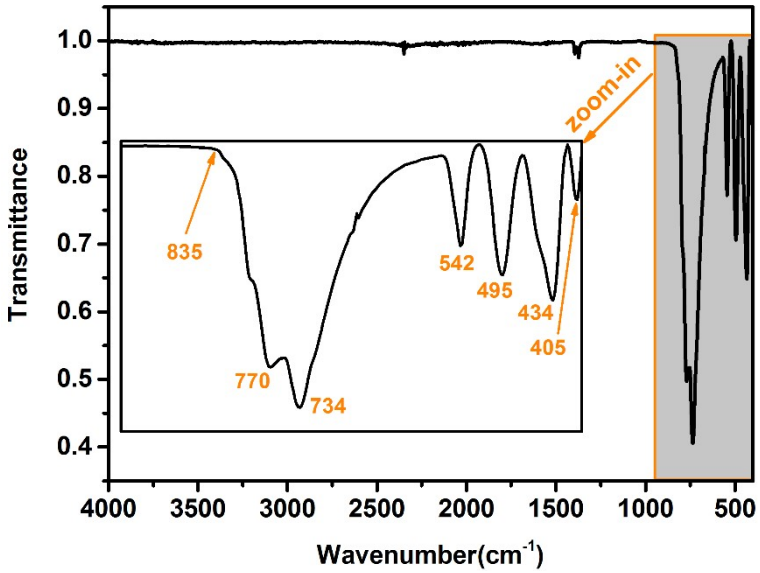

Figure S11. IR spectrum of $Ba_2[FeF_4(IO_3)_2]IO_3$, inset: zoomed-in view of IR bands.

(The IR absorption peaks of two compounds at 820−734 cm^{-1} and 542−405 cm^{-1} could be assigned to the symmetric and asymmetric stretching vibrations and bending vibrations of I−O bonds.)

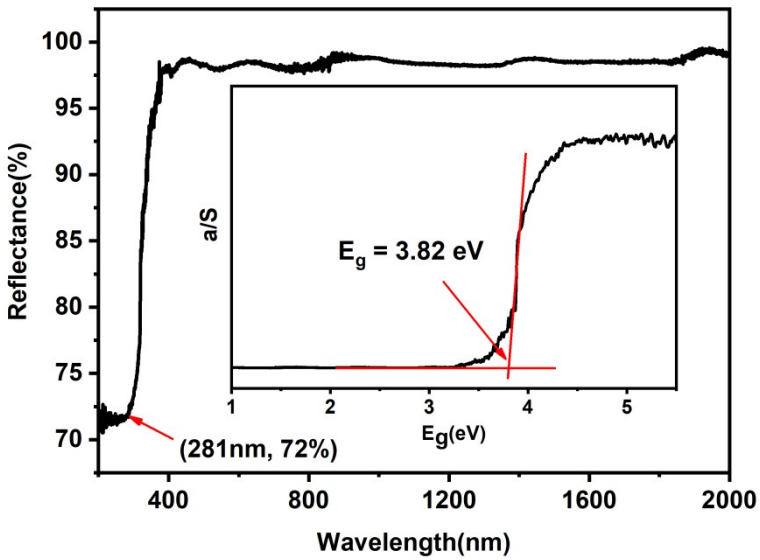

Figure S12 UV-vis-NIR spectrum of $Ba[FeF_4(IO_3)]$.

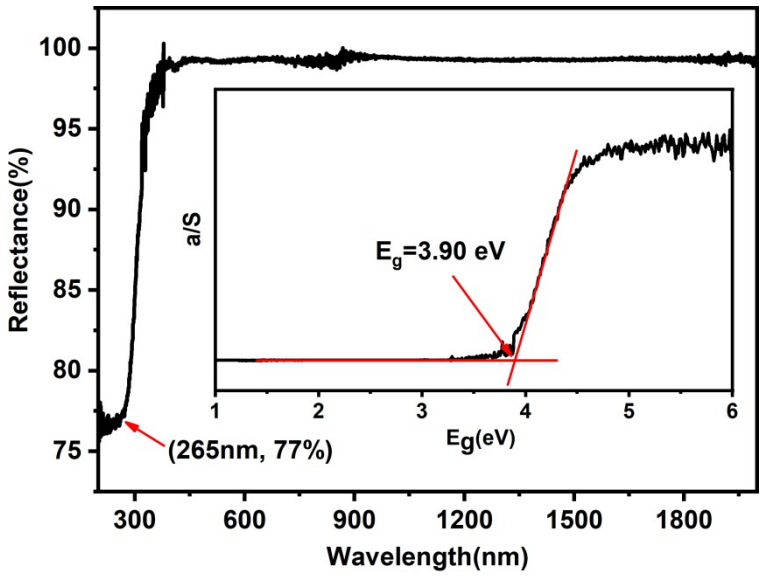

Figure S13 UV-vis-NIR spectrum of $Ba_2[FeF_4(IO_3)_2]IO_3$.

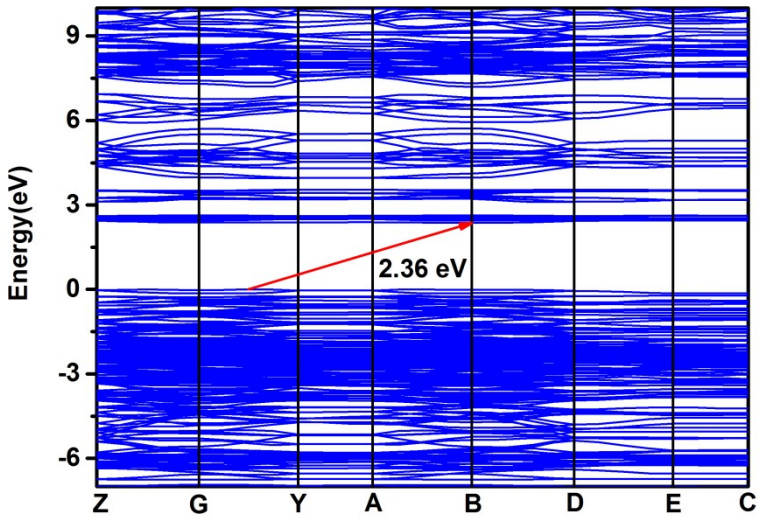

Figure S14. Calculated band structure of $Ba[FeF_4(IO_3)]$.

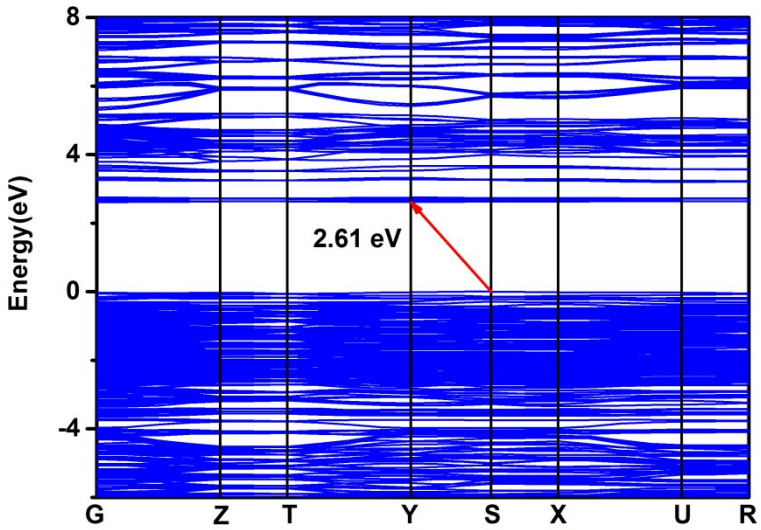

Figure S15. Calculated band structure of $Ba_2[FeF_4(IO_3)_2]IO_3$.

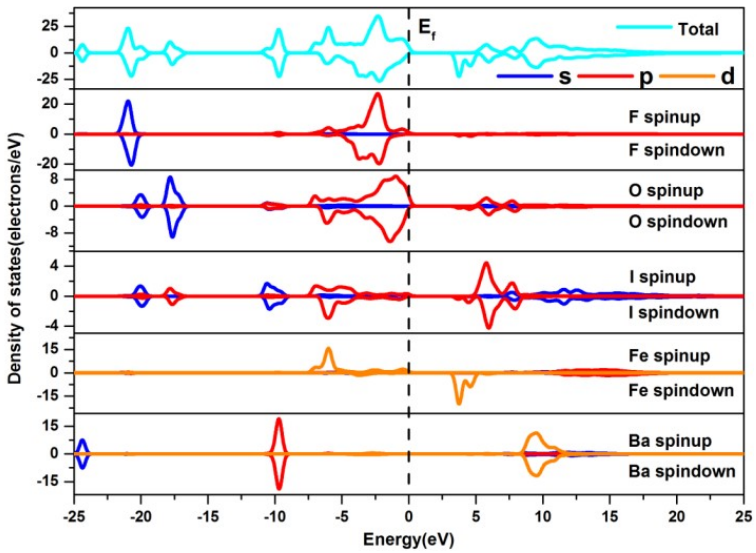

Figure S16. The scissor-added density of states for $Ba[FeF_4(IO_3)]$.

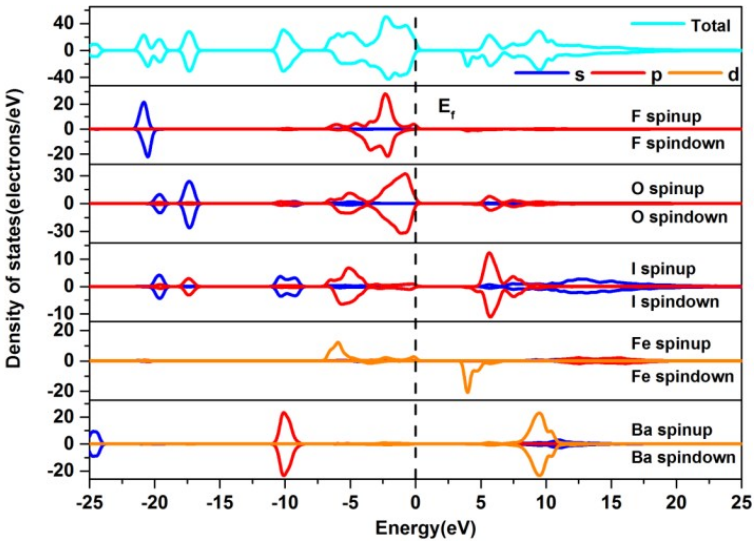

Figure S17. The scissor-added density of states for $Ba_2[FeF_4(IO_3)_2]IO_3$.

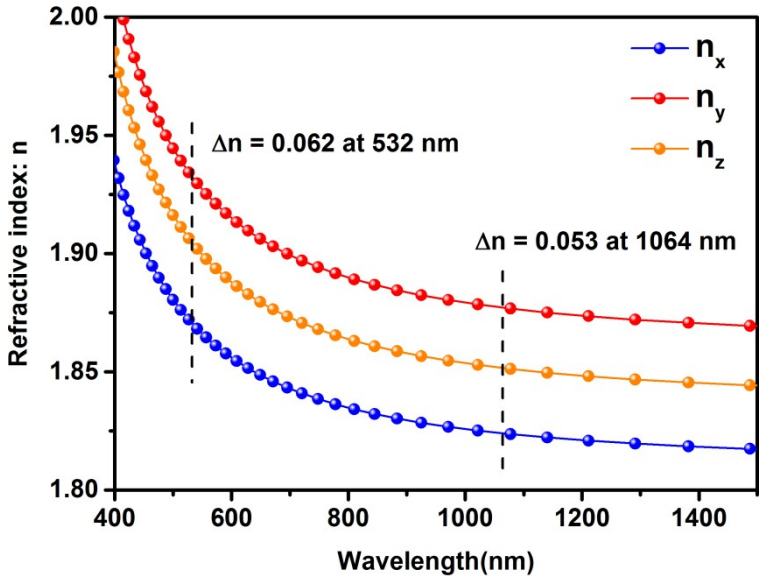

Figure S18. Calculated frequency-dependent refractive indices of $Ba[FeF_4(IO_3)]$.

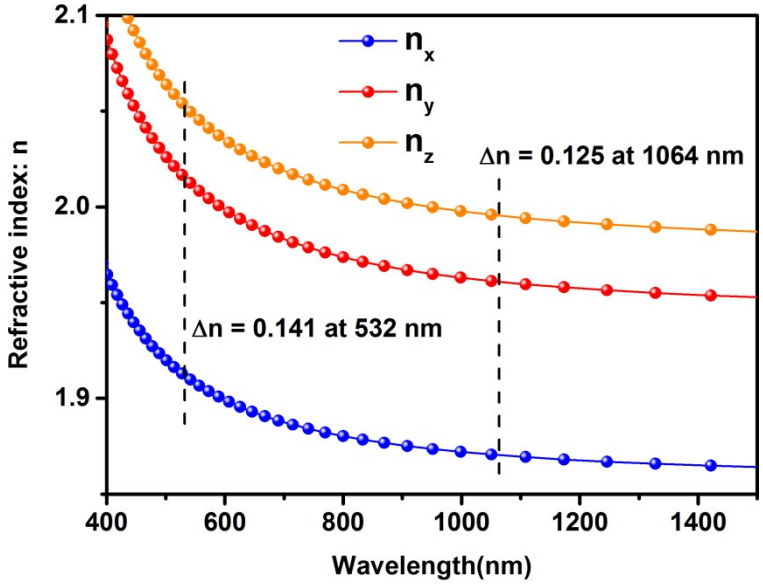

Figure S19. Calculated frequency-dependent refractive indices of $Ba_2[FeF_4(IO_3)_2]IO_3$.

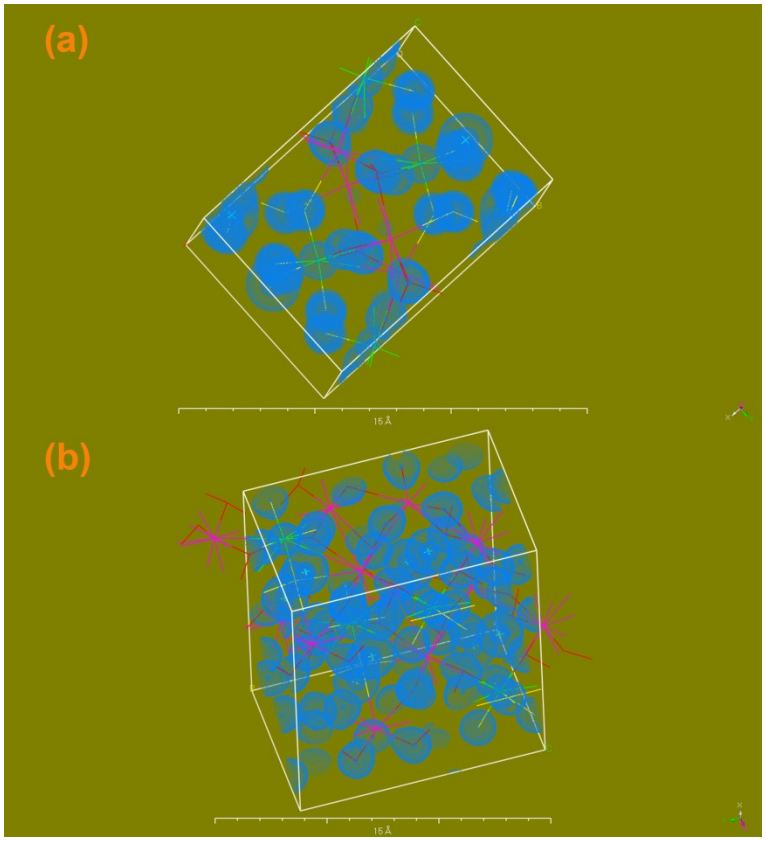

Figure S20. ELF diagrams of (a) $Ba[FeF_4(IO_3)]$ and (b) $Ba_2[FeF_4(IO_3)_2]IO_3$.

Reference

1. R. H. Blessing, *Acta Crystallogr., Sect. A: Found. Crystallogr.*, 1995, **51**, 33-38.
2. G. M. Sheldrick, *Acta Crystallogr A Found Adv*, 2015, **71**, 3-8.
3. G. M. Sheldrick, *Acta Crystallogr C Struct Chem*, 2015, **71**, 3-8.
4. A. L. Spek, *J. Appl. Crystallogr.*, 2003, **36**, 7-13.
5. H. D. Flack, *Acta Crystallogr., Sect. A: Found. Crystallogr.*, 1983, **39**, 876-881.
6. Kubelka and Munk, *Zeit. Für Tekn. Physik*, 1931, **12**, 593.
7. S. K. Kurtz and T. T. Perry, *J. Appl. Phys.*, 1968, **39**, 3798-3813.
8. V. Milman, B. Winkler, J. A. White, C. J. Pickard, M. C. Payne, E. V. Akhmatskaya and R. H. Nobes, *Int. J. Quantum Chem.*, 2000, **77**, 895-910.
9. M. D. Segall, P. J. D. Lindan, M. J. Probert, C. J. Pickard, P. J. Hasnip, S. J. Clark and M. C. Payne, *J Phys-Condens Mat*, 2002, **14**, 2717-2744.
10. J. P. Perdew, K. Burke and M. Ernzerhof, *Phys. Rev. Lett.*, 1996, **77**, 3865-3868.
11. J. S. Lin, A. Qteish, M. C. Payne and V. Heine, *Phys Rev B*, 1993, **47**, 4174-4180.